Articles

Solution Conformation of the *N*-(Deoxyguanosin-8-yl)-1-aminopyrene ([AP]dG) Adduct Opposite dC in a DNA Duplex†

Bing Mao,‡ Rajeev R. Vyas,§ Brian E. Hingerty,|| Suse Broyde,⊥ Ashis K. Basu,§ and Dinshaw J. Patel*,‡

Cellular Biochemistry and Biophysics Program, Memorial Sloan-Kettering Cancer Center, New York, New York 10021, Chemistry Department, University of Connecticut, Storrs, Connecticut 06269, Health Sciences Research Division, Oak Ridge National Laboratory, Oak Ridge, Tennessee 37831, and Biology Department, New York University, New York, New York 10003

Received May 6, 1996; Revised Manuscript Received July 12, 1996⊗

ABSTRACT: Combined NMR−molecular mechanics computational studies were undertaken on the C^8-deoxyguanosine adduct formed by the carcinogen 1-nitropyrene embedded in the d(C5-[AP]G6-C7)·d(G16-C17-G18) sequence context in a 11-mer duplex, with dC opposite the modified deoxyguanosine. The exchangeable and nonexchangeable protons of the aminopyrene moiety and the nucleic acid were assigned following analysis of two-dimensional NMR data sets in H_2O and D_2O solution. There was a general broadening of several proton resonances for the three nucleotide d(G16-C17-G18) segment positioned opposite the [AP]dG6 lesion site resulting in weaker NOEs involving these protons in the adduct duplex. The solution conformation of the [AP]dG·dC 11-mer duplex has been determined by incorporating intramolecular and intermolecular proton−proton distances defined by upper and lower bounds deduced from NOESY spectra as restraints in molecular mechanics computations in torsion angle space. The aminopyrene ring of [AP]dG6 is intercalated into the DNA helix between intact Watson−Crick dC5·dG18 and dC7·dG16 base pairs. The modified deoxyguanosine ring of [AP]dG6 is displaced into the major groove and stacks with the major groove edge of dC5 in the adduct duplex. Both carbon and proton chemical shift data for the sugar resonances of the modified deoxyguanosine residue are consistent with a *syn* glycosidic torsion angle for the [AP]dG6 residue. The dC17 base on the partner strand is displaced from the center of the helix toward the major groove as a consequence of the aminopyrene ring intercalation into the helix. This base-displaced intercalative structure of the [AP]dG·dC 11-mer duplex exhibits several unusually shifted proton resonances which can be accounted for by the ring current contributions of the deoxyguanosinyl and pyrenyl rings of the [AP]dG6 adduct. In summary, intercalation of the aminopyrene moiety is accompanied by displacement of both [AP]dG6 and the partner dC17 into the major groove in the [AP]dG·dC 11-mer duplex.

Nitroaromatic compounds are common environmental pollutants (Rosenkranz et al., 1980; Ohnishi et al., 1985; IARC, 1989). 1-Nitropyrene (1-NP),[1] a representative of this class of compounds, is the most abundant nitroaromatic compound found in many environmental samples. It has been detected in urban air particulate, coal fly ash, automobile exhaust, and grilled foods and in emissions from wood stoves, gas burners, and kerosene heaters (Rosenkranz et al., 1980; Tokiwa & Ohnishi, 1986; IARC, 1989). 1-NP is mutagenic in a variety of bacterial and mammalian systems (Rosenkranz & Mermelstein, 1983; Stanton et al., 1988; Yang et al., 1988, Newton et al., 1992) and is tumorigenic in experimental animals (El-Bayoumy et al., 1984; Hirose et al., 1984). Nitroreduction is a major pathway by which 1-NP is metabolized (Heflich et al., 1985). In both mammalian cells and bacteria, a major DNA adduct formed by 1-NP is *N*-(deoxyguanosin-8-yl)-1-aminopyrene ([AP]dG) **1** (Howard et al., 1983; Stanton et al., 1985). Recent studies

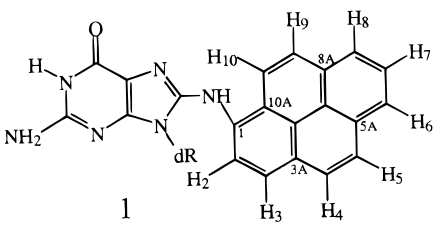

1

indicate that two additional deoxyguanosine adducts are formed, in which the covalent attachment occurs at the 6 or 8 position of the pyrene ring system with the N^2 position of deoxyguanosine (Herreno-Saenz et al., 1995). Despite the formation of multiple DNA adducts, the biological impor-

† This research is supported by NIH Grant CA-49982 to D.J.P., by NIH Grant ES-05695 to A.K.B., by NIH Grants CA-28038 and RR-06458 and DOE Grant DE-FG02-90ER60931 to S.B., and by DOE Contract DE-AC05-960R22464 with Lockheed Martin Energy Research and DOE OHER Field Work Proposal ERKP931 to B.E.H.

‡ Memorial Sloan-Kettering Cancer Center.

§ University of Connecticut.

|| Oak Ridge National Laboratory.

⊥ New York University.

⊗ Abstract published in *Advance ACS Abstracts,* September 1, 1996.

[1] Abbreviations: 1-NP, 1-nitropyrene; 1-NOP, 1-nitrosopyrene; NHOP, *N*-hydroxy-1-aminopyrene; AP, 1-aminopyrene; [AP]dG, *N*-(deoxyguanosin-8-yl)-1-aminopyrene; dG, 2′-deoxyguanosine; AF, 2-aminofluorene; AAF, *N*-acetyl-2-aminofluorene; ABP, 4-aminobiphenyl; BPDE, benzo[*a*]pyrene diol epoxide.

S0006-2960(96)01078-1 CCC: $12.00

tance of the C^8-[AP]dG adduct has been underscored by forward mutation assays in which it was introduced at random as the major DNA damage, and a dose-dependent mutagenic response was demonstrated (Melchior et al., 1994; Malia & Basu, 1995). In addition, a recent study employing a site-specific approach has unambiguously established that the C^8-[AP]dG induces frame-shift mutations in *Escherichia coli* (Malia et al., 1996). DNA polymerase stalling as a consequence of a C^8-[AP]dG adduct has also recently been demonstrated in an *in vitro* study (Vyas & Basu, 1995).

Several carcinogenic aromatic amines and amides form a similar group of C^8-dG adducts. Among these the most extensively studied adducts are the ones generated by 2-aminofluorene (AF), 2-acetylaminofluorene (AAF), and 4-aminobiphenyl (ABP) [for reviews see Beland and Kadlubar (1985, 1990)]. The biological effect of each of these aromatic amines is distinct. It is widely believed that the three-dimensional structural effects induced by the C^8-dG adducts of these aromatic amines on DNA architecture are likely associated with differences in their biological effects.

The C^8-dG adduct formed by AAF induces a rotation of the glycosidic torsion angle of the base from the normal *anti* domain in B-DNA to *syn* accompanied by local denaturation of the [AAF]dG·C base pair with displacement of the modified dG and insertion of the AAF moiety into the helix. This model, termed base displacement (Grunberger et al., 1970) or insertion−denaturation (Fuchs & Daune, 1971), was supported by early data, summarized in Singer and Grunberger (1983). A recent high-resolution NMR study has confirmed these models (O'Handley et al., 1993). In addition, in alternating G−C sequences the *syn* conformation of the AAF-modified deoxyguanosine facilitates the B to Z conversion of DNA (Santella & Grunberger, 1983). A large number of genetic studies on AAF indicate that the major type of mutation induced by AAF-adducts are frame-shifts occurring mainly in strings of G·C base pairs [Fuchs et al., 1981; reviewed in Heflich and Neft (1994)].

By contrast, AF-induced mutations are mainly base-pair substitutions, predominantly G·C to T·A transversions [Bichara & Fuchs, 1985; reviewed in Heflich and Neft (1994)]. In the case of the C^8-dG adduct of AF, the glycosidic torsion angle of the modified base can be either *anti* or *syn*. A number of different structural themes have been observed for this adduct depending on the context. With dA, dG, or dI opposite C^8-[AF]dG, high-resolution NMR studies reveal that the adducted dG is rotated to *syn* and the aminofluorene ring is located in the minor groove (Norman et al., 1989; Abuaf et al., 1995). In these structures, there is no hydrogen bond between the adducted dG and the mismatched base on the partner strand at physiological pH, but the pair remains stacked within the helix. By contrast, AF adducts, recently studied by high-resolution NMR in the contexts of −1 and −2 deletion duplexes in which the adducted dG, or the adducted dG and its 3′ neighbor, has no partner (Mao et al., 1995a,b), reveal a different structural theme. In both of these deletion duplexes the aminofluorene ring is inserted into the helix at the deletion site; the adducted dG is also in a *syn* alignment, but it is displaced into the major groove. In normal duplexes with dC opposite the modification site, high-resolution NMR studies reveal a conformational equilibrium (Cho et al., 1994; Eckel & Krugh, 1994). In one conformer the AF is in the B-DNA major groove, with all base pairs intact and the modified deoxyguanosine glycosidic torsion angle in the *anti* domain. The second conformer has the AF inserted into the helix with denaturation at the lesion site and displacement of the modified base, which is assumed to adopt the *anti* conformation (Eckel & Krugh, 1994).

The C^8-dG adduct of 4-aminobiphenyl (ABP) resembles the AF adduct when studied in the same sequence context (Cho et al., 1992). It was studied in the same 15-mer duplex with dC opposite the modified dG as the AF adduct (Cho et al., 1994). In the ABP adduct, the glycosidic torsion angle of the major conformer is *anti* and the arylamine moiety resides in the major groove in a weakly distorted double helix. There appears to be a minor conformer in which the ABP moiety may be stacked with the neighboring base pairs or reside in the minor groove. Like AF, ABP also induces dG·dC to dT·dA transversions (Melchior et al., 1994).

The structure and mutagenic studies of the C^8-dG adducts of AAF, AF, and ABP, taken together, suggest that the structure of the carcinogen as well as the local DNA sequence context plays crucial roles in governing the conformation of DNA adducts, which in turn may govern their biological effect. However, in comparison to these aromatic amine adducts, relatively little is known about the structural effect of the bulkier [AP]dG adduct. A recent investigation using optical spectroscopic techniques in a d(T-[AP]G-A) sequence context suggested the presence of one or more conformers of the adduct in which the aminopyrene residue is in a quasi-intercalative orientation, as well as one(s) in which it is externally bound (Nolan et al., 1996). Despite the presence of multiple conformations, relatively little destabilization of the duplex was observed. Thermal melting studies, which provide a measure of the extent of helix stability in relation to the unmodified sequence, show that the stability of the modified duplex is comparable to the unmodified one, with a computed free energy difference of only 1.2 kcal/mol in favor of the unmodified structure. However, attempts to study this sequence by NMR were unsuccessful, presumably due to the existence of multiple conformations. In the current work, we have studied the solution structure of the [AP]dG adduct **1** opposite dC in the d(C-[AP]G-C) sequence context **2** in a 11-mer duplex. This same 11-mer sequence has been

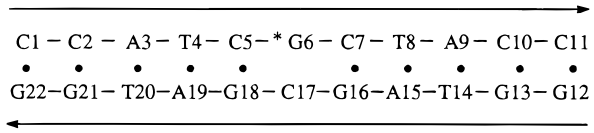

2

employed previously by us in structural studies of a variety of lesions including the N^2-dG adducts formed by the stereoisomeric diol epoxides of benzo[*a*]pyrene and 5-methylchrysene (Cosman et al., 1992; de los Santos et al., 1992; Cosman et al., 1993a, 1994a,b, 1995a) as well as the C^8-dG adduct formed by AF (Mao et al., 1995a). Our results show that the dG ring of [AP]dG is in a *syn* alignment and displaced into the major groove. The aminopyrene ring is intercalated in its place, between the two intact adjacent dG·dC base pairs; the dC base located opposite the adduct on the partner strand is also displaced from the center of the helix toward the major groove. This 11-mer duplex exhibits

several unusually shifted proton resonances, which can be accounted for by the ring current contributions of the deoxyguanosinyl and pyrenyl rings of the [AP]dG adduct. Similarities between this and other base-displaced intercalation structures suggest that a conformer of this type may represent an intermediate in frame-shift mutagenesis.

MATERIALS AND METHODS

Oligonucleotide Synthesis and Adduct Formation. The deoxyoligonucleotides d(C-C-A-T-C-G-C-T-A-C-C) and d(G-G-T-A-G-C-G-A-T-G-G) were synthesized on an Applied Biosystems model 392 DNA synthesizer and purified by reverse-phase HPLC.

Preparation and purification of the [AP]dG containing the 11-mer were carried out as reported previously (Vyas et al., 1993; Nolan et al., 1996). The d(C-C-A-T-C-[AP]G-C-T-A-C-C) 11-mer strand was annealed with the complementary d(G-G-T-A-G-C-G-A-T-G-G) 11-mer strand at 1 °C, and the stoichiometry was followed by monitoring proton resonances on both strands.

Sample Preparation. The NMR spectra of the [AP]dG·dC 11-mer duplex (3 mM in duplex) were recorded in 0.1 M NaCl, 10 mM phosphate, 1 mM EDTA solution containing either D_2O or 90:10 H_2O/D_2O (v/v). All NMR spectra were recorded on samples at pH 7.0.

NMR Experiments. All NMR data sets were recorded on Varian Unity Plus 500 and 600 MHz NMR spectrometers. A combination of through-space nuclear Overhauser effect (NOESY) and through-bond correlated (COSY, TOCSY) two-dimensional spectra were recorded and analyzed to assign the aminopyrene and nucleic acid protons in the [AP]-dG·dC 11-mer duplex. NOESY spectra (150 ms mixing time) of the modified duplex spectra in H_2O buffer were collected at 1 °C using an optimized jump−return pulse sequence for solvent suppression. The corresponding NOESY spectra in D_2O buffer were collected as a function of mixing time at 25 °C. The through-bond TOCSY spectra were recorded in D_2O buffer at spin lock times of 40 and 80 ms at 25 °C.

The indirect detected proton−phosphorus correlation spectrum was recorded on the [AP]dG·dC 11-mer duplex in D_2O at 25 °C using the pulse sequence described by Sklenar et al. (1986). Both proton and phosphorus spectral widths were set to 6 ppm in both dimensions with a 1.3 s presaturation of the residual HOD resonance. The phosphorus spectra were referenced relative to external 10% (v/v) trimethyl phosphate (TMP) sample.

A proton−carbon HMQC correlation spectrum on the [AP]-dG·dC 11-mer duplex was recorded in D_2O buffer at 25 °C. The proton carrier frequency was set to 4.5 ppm with a spectral width of 8.5 ppm, while the ^{13}C carrier frequency was set to 67.0 ppm with a spectral width of 66.0 ppm. The carbon spectra were referenced relative to external 3-(trimethylsilyl)propionate (TSP) using the method described by Bax and Subramanian (1986).

The volume integrals of NOE cross-peaks as a function of five mixing times (50, 80, 100, 150, and 200 ms) were measured to generate the build-up curves for nonexchangeable protons in D_2O solution. The interproton distances were calculated based on the two-spin approximation using the dT(NH3)-dA(H2) fixed distance of 2.92 Å for NOESY data sets in H_2O and the dC(H5)-dC(H6) fixed distance of 2.45 Å for NOESY data sets in D_2O solution. A quadratic polynomial was fitted to the data points, and the initial slope was calculated from the linear fit of the quadratic curves to the first non-zero mixing time. The upper and lower bound ranges of the estimated interproton distances for nonexchangeable protons were determined on the basis of the resolution of the cross-peaks in the two-dimensional contour plots and the quality of the NOE build-up plots. However, the cross-peaks between protons located at or close to the lesion site were broad in the [AP]dG·dC 11-mer duplex. In these cases, the distance restraints were estimated from counting the number of NOE cross-peak contours present at both short (50 ms) and long (300 ms) mixing times and categorizing the restraints as strong (2.2−3.5 Å), medium (3.0−4.5 Å), and weak (4.0−6.0 Å).

The base proton to sugar H1′ proton NOE cross-peaks in the shortest mixing time NOESY data set in D_2O were evaluated to qualitatively differentiate between *syn* (strong NOE) and *anti* (weak NOE) glycosidic torsion angles (Patel et al., 1982). The proton−proton vicinal coupling constants among sugar protons were analyzed from phase-sensitive COSY spectra to qualitatively distinguish between the C3′-*endo* and C2′-*endo* family of sugar puckers. The relative intensity of the NOE cross-peaks between base protons and their own and 5′-flanking sugar H2′, H2″, and H3′ protons were also used to qualitatively distinguish between the A-DNA and B-DNA family of helices for the modified duplex (van der Ven & Hilbers, 1988).

Molecular Mechanics Computations. Minimized potential energy calculations were carried out with DUPLEX, a molecular mechanics program for nucleic acids that performs potential energy minimizations in the reduced variable domain of torsion angle space (Hingerty et al., 1989). DUPLEX uses a potential set similar to the one developed by Olson and co-workers for nucleic acids (Taylor & Olson, 1983). Force field parameters, including partial charges, for the [AP]dG adduct were the same as those employed previously (Nolan et al., 1996). The geometry of the [AP]-dG adduct was also the same as described earlier (Nolan et al., 1996). A hydrogen-bond penalty function (Hingerty et al., 1989) was employed in all first-stage minimizations to aid the minimizer in locating the Watson−Crick hydrogen-bonded structures indicated by the NMR data. To locate minimum energy conformations with interproton distances available from the experimental NMR data, pseudo-potentials (permitting upper and lower bound restraints) were added to the energy, as described previously (Norman et al., 1989; Schlick et al., 1990; Cosman et al., 1993). Briefly, the following functions were used:

$$F_N = W_N \sum_1^n (d - d_N)^2 \quad (1)$$

$$F_{NN} = W_{NN} \sum_1^n (d - d_{NN})^2 \quad (2)$$

The W's are adjustable weights (in the range 10−30 kcal/mol Å^2), d is the current value of the interproton distance, d_N is a target upper bound, and d_{NN} a target lower bound. Equation 1 is implemented when d is greater than d_N, and eq 2 is implemented when d is less than d_{NN}. The functions are summed over all n target distances. All penalty functions

were released in the last minimization steps to yield unrestrained final structures that are minimum energy conformations. F_N and F_{NN} can also be employed as relative indices of goodness-of-fit to the NMR data. Here the *d* values are the achieved distances in a given model, and the *W*'s are the weights employed in the search. F_N and F_{NN} are composites, reflecting the overall fit of all the achieved distances to their targets. They both adopt values of zero when all model distances are within the upper and lower NMR distance bounds. Small deviations from the NMR targets, within the uncertainty of the data, are accepted in computed models, and these therefore have non-zero F_N and F_{NN} values. Computations were carried out at the Department of Energy's National Energy Research Supercomputer Center and the National Science Foundation's San Diego Supercomputer Center.

Our search strategy employs a set of key NMR distance restraints, together with information from the NMR data on the hydrogen bonding pattern between bases for the hydrogen bond penalty function. NMR information about the glycosidic torsion angle and the deoxyribose sugar pseudorotation parameter are also included. The resulting structures are ranked according to energy and goodness-of-fit (eqs 1 and 2). At this point the first set of NMR assigned distance bounds are evaluated in relation to achieved distances and energies in the ensemble of 16 structures. Cross-checks involving distances not employed as restraints and satisfaction of other criteria such as chemical shifts are also made. Especially in the case of conformational heterogeneity, this affords feedback to the NMR analysis and offers the opportunity for reassessment of the distance bounds. This procedure can be carried out iteratively until structures of lowest energy and best goodness-of-fit are located.

RESULTS

Exchangeable Proton Spectra. The one-dimensional proton NMR spectrum of the [AP]dG·dC 11-mer duplex in H_2O buffer solution at 1 °C is plotted in Figure 1A. Several partially resolved imino resonances between 12.5 and 14.0 ppm and two upfield-shifted resonances at 11.26 and 11.47 ppm (Figure 1A) are observed in the spectrum. The imino protons have been assigned following an analysis of the 150 ms mixing time NOESY spectrum in H_2O buffer solution at 1 °C (Figure 2). The connectivities between adjacent base pairs in the 11-mer duplex segment can be readily traced from the dC11·dG12 pair located at one end of the helix to the dC2·dG21 pair located at the opposite end of the duplex (Figure 2B) with no NOE detected between the two upfield-shifted imino protons of dG16 and dG18 (Figure 2B).

An expanded plot of the 150 ms mixing time NOESY spectrum of the [AP]dG·dC 11-mer correlating connectivities between the imino protons (11.0−14.0 ppm) and the base and amino protons (4.8−8.8 ppm) is plotted in Figure 2A. The Watson−Crick base-pairing alignments for the dC5·dG18 and dC7·dG16 base pairs of the duplex segment nearest to the [AP]dG residue are intact, as demonstrated by the presence of the cross-peaks between dG16(NH1) and dC7-(NH_2-4b,e) (peaks A and A′, Figure 2A) and between dG18-(NH1) and dC5(NH_2-4b,e) (peaks B and B′, Figure 2A). The Watson−Crick base-pairing alignments for the remaining four dA·dT and four dG·dC base pairs in the 11-mer duplex segment remain intact and unperturbed, as shown by the cross-peaks between thymine imino and deoxyadenosine H2 protons across the dA·dT pairs and between deoxyguanosine imino and deoxycytidine amino protons across the dG·dC pairs (Figure 2A).

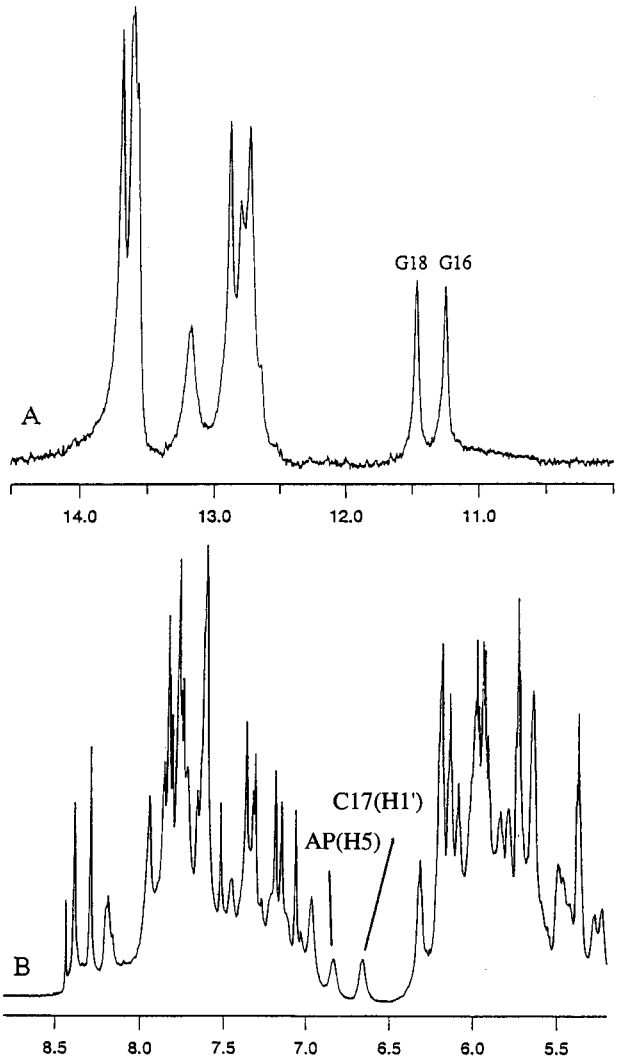

FIGURE 1: (A) Imino proton spectrum (10.0−14.5 ppm) of the [AP]-dG·dC 11-mer duplex at 1 °C and (B) nonexchangeable proton spectrum (5.2−8.7 ppm) of the [AP]dG·dC 11-mer duplex at 25 °C. The imino proton assignments of dG16 and dG18 are listed over the resonances in the spectrum in A.

The two upfield-shifted imino protons (11.26 and 11.47 ppm) are assigned to dG16 and dG18, respectively. In addition to the unusual upfield shift of the dG16 and dG18 imino protons, we observed intermolecular NOEs between these imino protons and aminopyrene protons (peaks 1−4 in Figure 2A) in the [AP]dG·dC 11-mer duplex.

The [AP]G6 imino proton was not observed, which suggests that the [AP]G6 is most likely not hydrogen-bonded with its partner dC17 in the adduct duplex and that its exposed imino proton rapidly exchanges with H_2O.

The exchangeable proton chemical shifts for the central d(C5-[AP]G6-C7)·d(G16-C17-G18) segment of the [AP]-dG·dC 11-mer duplex are listed in Table 1 and for the entire adduct duplex in supplementary Table S1.

Exchangeable proton chemical shift differences for the central segment between the adduct duplex and the control duplex are given in supplementary Table S2. Large upfield shifts are observed for the imino protons of flanking dG16

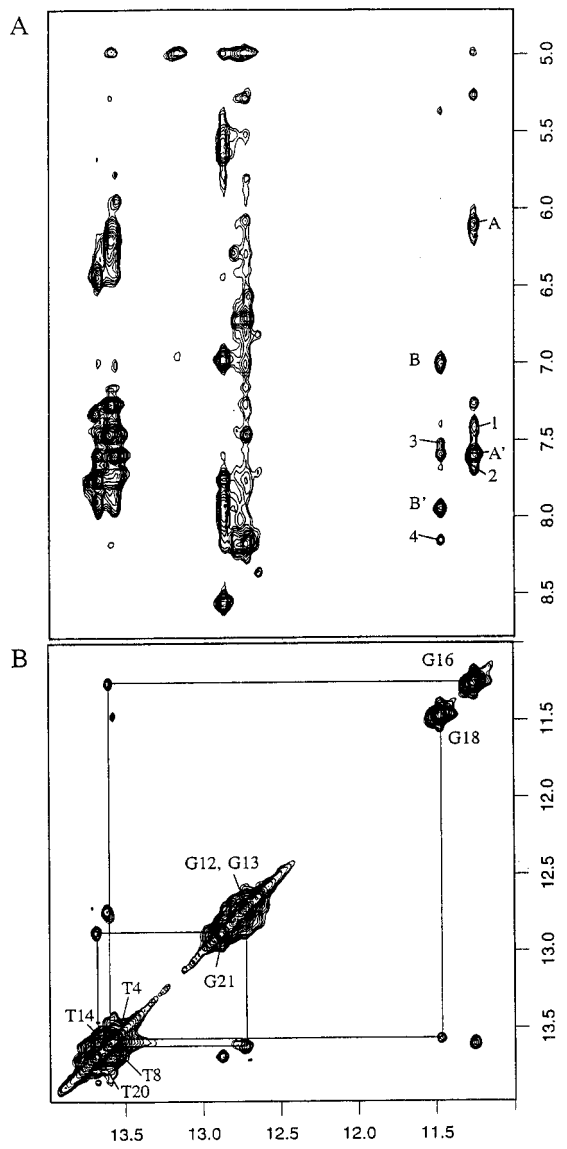

FIGURE 2: Expanded NOESY (150 ms mixing time) contour plots of the [AP]dG·dC 11-mer duplex in H_2O buffer at 1 °C. (A) Expanded plot of the NOE connectivities between the imino protons (11.0−14.0 ppm) and the base and amino protons (4.7−8.8 ppm) region. The NOE cross-peaks involving the imino protons are labeled in the figure as follows: A, A′, G16(NH1)-C7(NH_2-4e,b); B, B′, G18(NH1)−C5(NH_2-4e,b). The intermolecular NOE cross-peaks 1−4 are assigned as follows: 1, G16(NH1)-AP(H10); 2, G16-(NH1)−AP(H8); 3, G18(NH1)-AP(H3); and 4, G18(NH1)-AP(H2). (B) Expanded plot of the NOE connectivities within the symmetrical imino proton (11.0−14.0 ppm) region.

and dG18 and the amino protons of flanking dC5 and dC7 on [AP]dG6 adduct formation.

Nonexchangeable Proton Spectra. The nonexchangeable proton spectrum (5.2−8.7 ppm) of the [AP]dG·dC 11-mer duplex in D_2O buffer at 25 °C is plotted in Figure 1B. The nucleic acid base and sugar protons, as well as the aminopyrene protons, were assigned on the basis of an analysis of through-space distance connectivities in NOESY data sets as a function of mixing time and through-bond connectivities in COSY and TOCSY data sets recorded in D_2O buffer, pH 7.0 at 25 °C.

The expanded NOESY (300 ms mixing time) contour plot establishing sequential connectivities between the base protons and the sugar H1′ and cytosine H5 protons of the adduct duplex in D_2O buffer, pH 7.0 at 25 °C, is plotted in Figure 3. The NOE connectivities from the base (purine H8/pyrimidine H6) proton to its own and 5′-flanking sugar H1′ protons have been traced along the duplex from dC1 to dC11 on the modified strand and from dG12 to dG22 on the complementary strand. This tracing is shown for the central segment extending from dA3 to dA9 on the modified strand (solid line, Figure 3) and from dT14 to dT20 on the unmodified complementary strand (dashed line, Figure 3). The interruption in the tracing at the dC5-[AP]dG6 step on the modified strand is due to the absence of a purine H8 proton following aminopyrenyl modification at the C^8 position of dG6 in the adduct duplex. Some cross-peaks are not observed or are very weak at the dG16-dC17-dG18 step on the unmodified complementary strand, and the H1′ proton of dG18 is not observed (Figure 3). This most likely reflects the broad resonances for these residues in the [AP]-dG·dC 11-mer adduct duplex. The base and sugar H1′ proton assignments have been confirmed by cross-checks in other regions of the NOESY contour plot, as well as from COSY and TOCSY plots to also yield the sugar H2′, H2″, H3′, and H4′ proton assignments for the [AP]dG·dC 11-mer duplex.

The nonexchangeable proton chemical shifts for the central d(C5-[AP]G6-C7)·d(G16-C17-G18) segment in the [AP]dG·dC 11-mer duplex are listed in Table 1, and those for the entire adduct duplex are listed in supplementary Table S3. Nonexchangeable proton chemical shift differences for the central segment between the adduct duplex and the unmodified control duplex are given in supplementary Table S2.

It should be noted that relative to the control duplex, upfield shifts are observed on adduct formation at several base and major groove sugar protons of the dC5 residue located 5′ to the lesion site on the modified strand. These results suggest that the modified deoxyguanosine ([AP]dG6) is most likely displaced into the major groove and stacked over the dC5 residue. By contrast, downfield chemical shift differences are observed on adduct formation at the base and sugar protons of the dC17 residue (Table S2). This suggests that the dC17 residue positioned opposite the lesion site is most likely looped out of the helix and no longer stacked with the neighboring base pairs. In addition, downfield shifts are also observed on adduct formation at the sugar protons of the [AP]dG6 residue (Table S2). Further, we observe an inversion in the characteristic H2′ and H2″ sugar cross-peak patterns at the lesion site with the H2′ proton (3.51 ppm) of [AP]dG6 shifting dramatically downfield in the adduct duplex (Figure 4).

Aminopyrene Protons. The nonexchangeable aminopyrene protons were assigned from an analysis of through-space and through-bond two-dimensional spectra of the [AP]dG·dC 11-mer duplex recorded in D_2O buffer, pH 7.0 at 25 °C. The NOE connectivities can be traced starting from the H2 proton and proceeding to the H10 proton within the aminopyrene ring in the 300 ms NOESY spectrum of the adduct duplex (Figure 5A). The H2 and H10 protons can be differentiated following analysis of coupling patterns observed in COSY and TOCSY (Figure 5B) spectra. The exchangeable aminopyrene NH proton was not observed in the spectrum of the adduct duplex. The nonexchangeable aminopyrene proton chemical shifts in the [AP]dG·dC 11-mer duplex are listed in the caption to Figure 5.

Table 1: Proton and Phosphorus Chemical Shifts of the d(C5-[AP]G6-C7)·d(G16-C17-G18) Segment of the [AP]dG·dC 11-Mer Duplex in Aqueous Buffer

	Exchangeable Proton Chemical Shifts (ppm, 1 °C)		
		G(NH1)	*C*(NH_2-4)
dC5·dG18		11.47	7.01,[a] 7.95[b]
[AP]dG6·dC17		na[c]	
dC7·dG16		11.26	6.11,[a] 7.60[b]

	Nonexchangeable Proton and Phosphorus Chemical Shifts (ppm, 25 °C)						
	H8/H6	H2/H5	H1′	H2′, H2″	H3′	H4′	^{31}P[d]
dC5	6.96	5.35	5.77	1.04, 2.25	4.42	4.18	−3.90
[AP]dG6			6.08	3.51, 2.56	5.22	4.23	−3.28
dC7	7.72	5.36	5.99	2.21, 2.40	4.85	4.31	−4.10
dG16	6.96		5.27	2.10, 2.32	4.96	4.22	−3.17
dC17	7.96	6.13	6.66	2.45, 2.63	5.09	4.49	−4.15
dG18	7.60		na	na, na	4.51	4.12	−4.27

[a] Exposed amino proton. [b] Hydrogen-bonded amino proton. [c] na, not assigned. [d] ^{31}P chemical shift corresponds to residue (*n*) for the (*n*)-^{31}P-(*n*+1) step.

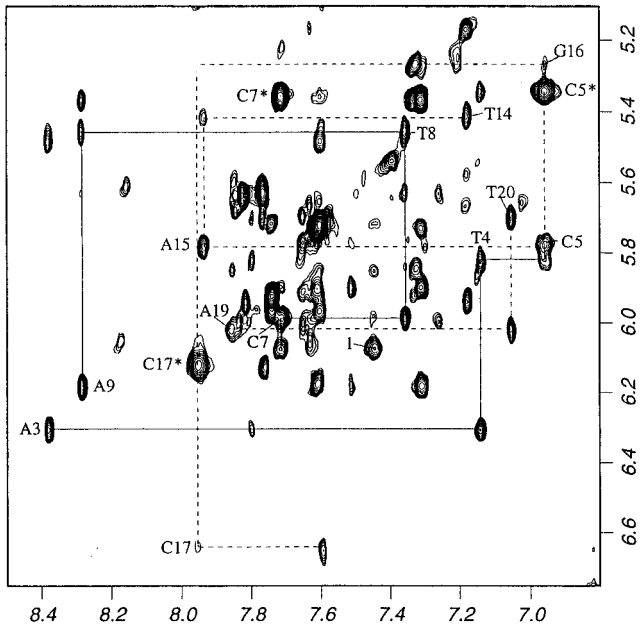

FIGURE 3: Expanded NOESY (300 ms mixing time) contour plot of the [AP]dG·dC 11-mer duplex in D_2O buffer at 25 °C establishing distance connectivities between the base protons (6.8−8.5 ppm) and the sugar H1′ and deoxycytidine H5 protons (5.1−6.7 ppm). The NOE connectivities between the base and their own and the 5′-flanking sugar H1′ protons from dA3 to dT8 on the modified strand are shown by solid lines, and those from dT14 to dT20 on the unmodified partner strand are shown by dashed lines. The assignments label the base to their own sugar H1′ NOEs, while the deoxycytidine H6-H5 NOEs are designated by asterisks. The carcinogen−DNA NOE cross-peak 1 is assigned to [AP]-G6(H1′)-AP(H10).

Carcinogen−DNA NOEs and Restraints. We observe a set of carcinogen−DNA NOEs centered about the lesion site in the [AP]dG·dC 11-mer duplex which have been categorized on the basis of whether they involve exchangeable or nonexchangeable protons. The corresponding carcinogen−DNA distance restraints deduced from NOE build-up curves for nonexchangeable protons and defined by lower and upper bounds in the [AP]dG·dC 11-mer duplex are listed in Table 2.

The observed NOEs between the aminopyrene H2, H3, H8, and H10 protons and the imino protons of dG16 and dG18 place the aminopyrene between the dC5·dG18 and dC7·dG16 base pairs in the adduct duplex. We observe NOEs between the aminopyrene H5 and H6 protons at the [AP]dG6 lesion site and the sugar H2′ and H2″ protons of dG16, as well as between the aminopyrene H6 proton and sugar H4′ proton of dC17 in the adduct duplex (supplementary Figure S1). These NOEs establish that the aminopyrene ring edge furthest from the covalent linkage site is positioned near the base and sugar protons of dG16 and dC17 on the partner strand of the [AP]dG·dC 11-mer duplex. The long axis of the aminopyrene ring must be approximately parallel to the long axis of the flanking base pairs if its H5 and H6 protons are to interact with the partner strand across from the lesion site.

Carbon Spectra. The expanded contour plot of a natural abundance proton-carbon HMQC correlation experiment that correlates the H1′ and C1′ chemical shifts of individual residues for the [AP]dG·dC 11-mer duplex in D_2O buffer, pH 7.0 at 25 °C, is plotted in Figure 6A. The carbon resonances are assigned on the basis of the known H1′ proton assignments in the adduct duplex. The C1′ chemical shift assignments for residues in the d(T4-C5-[AP]G6-C7-T8)·d(A15-G16-C17-G18-A19) segment together with all guanine residues in the adduct duplex are labeled in Figure 6A except for dG16, dC17, and dG18 residues due to the broad nature of their resonances. We note that the C1′ chemical shift of [AP]dG6 (88.91 ppm) is ∼3 ppm downfield of other assignable dG residues which are observed to resonate between 84.5 and 86.5 ppm in the adduct duplex (Figure 6A). It has been previously established that downfield sugar C1′ carbon chemical shifts that can range up to 5 ppm are observed for DNA residues adopting *syn* glycosidic torsion angles provided that they retain C2′-*endo* sugar pucker geometries (Ghose et al., 1994; Greene et al., 1995). We detect a strong coupling cross-peak between the H1′ (5.68 ppm) and H2′ (3.11 ppm) protons of [AP]dG6 (Figure 4B) placing this sugar within the C2′-*endo* range. The ∼3 ppm downfield sugar C1′ carbon chemical shift of [AP]dG6 identifies a *syn* glycosidic torsion angle at this modified residue in the [AP]dG·dC 11-mer duplex.

Phosphorus Spectra. The proton decoupled phosphorus spectrum of the [AP]dG·dC 11-mer duplex has been recorded in D_2O buffer, pH 7.0 at 25 °C. The phosphorus resonances are dispersed over a 1.5 ppm range with several resonances shifted to low field of the −4.0 to −4.5 ppm spectra region characteristic of an unperturbed B-DNA phosphodiester

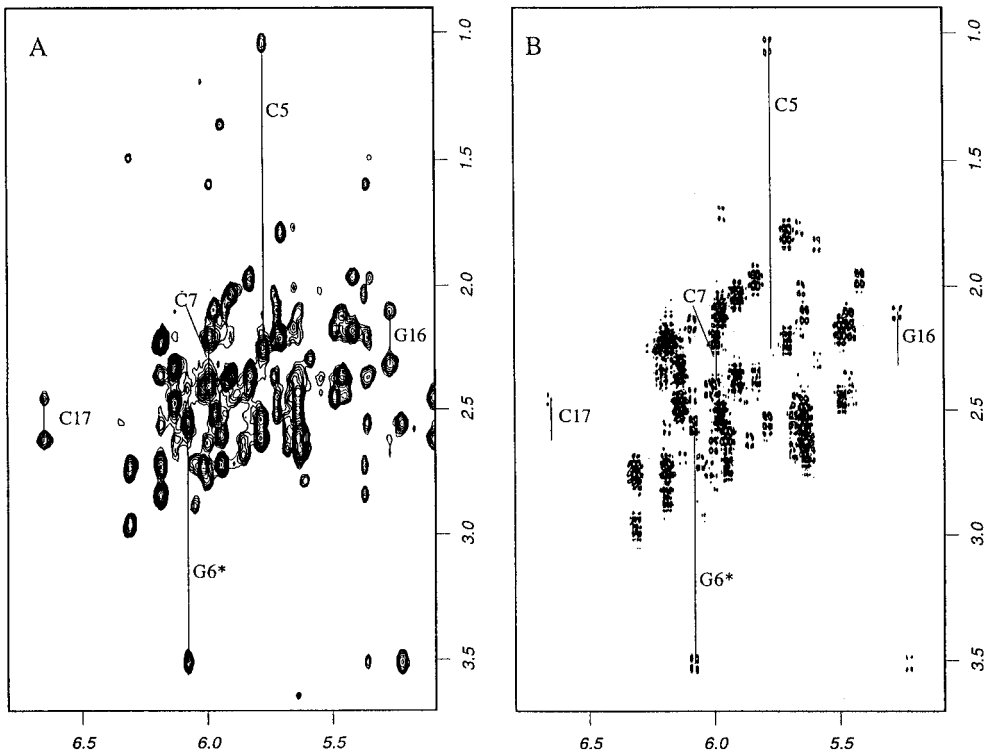

FIGURE 4: (A) Expanded NOESY (300 ms mixing time) contour plot of the [AP]dG·dC 11-mer duplex in D_2O buffer at 25 °C showing NOEs between the sugar H1′ protons (5.1−6.8 pm) and H2′,H2″ protons (0.9−3.7 ppm). (B) Expanded phase-sensitive COSY contour plot of the [AP]dG·dC 11-mer duplex in D_2O buffer at 25 °C establishing coupling connectivities between the H1′ protons (5.1−6.8 ppm) and H2′,H2″ protons (0.9−3.7 ppm). In both A and B the H2′ and H2″ protons of dC5, [AP]dG6, dC7, dG16, and dC17 are connected by lines and labeled. The H2′ protons resonate upfield of the H2″ protons for the majority of these residues except for [AP]dG6 where the H2″ proton resonates upfield of the H2′ proton. Notice the unusual upfield shift of the H2′ proton of C5 and the unusual downfield shift of the H2′ proton of [AP]dG6.

backbone. The phosphorus resonances have been assigned from an analysis of the proton-detected phosphorus−proton heteronuclear correlation experiment with the expanded contour plot shown in Figure 6B. Each phosphorus resonance can be correlated to the 5′-linked H3′ proton and the 3′-linked H4′ and H5′,5″ protons. The phosphorus resonances are assigned on the basis of the known H3′ and H4′ proton assignments in the adduct duplex. The phosphorus assignments for the individual steps in the d(T4-C5-[AP]-G6-C7-T8)·d(A15-G16-C17-G18-A19) segment of the adduct duplex are labeled in Figure 6B and listed in Table 1. The phosphorous chemical shifts for the [AP]dG6-dC7 (−3.28 ppm) and dG16-dC17 (−3.17 ppm) steps are shifted to low field of the −4.0 to −4.5 ppm unperturbed phosphodiester backbone chemical shift range.

Molecular Mechanics Computations. The search strategy employed began with a B-DNA (Arnott et al., 1976) central d(T4-C5-[AP]G6-C7-T8)·d(A15-G16-C17-G18-A19) base pair segment of the [AP]dG·dC 11-mer duplex. The computations were guided by the carcinogen−DNA and DNA−DNA restraints listed in Table 2 and supplementary Table S4, respectively. The AP−DNA orientation space was searched with 16 energy minimization trials in which the linkage torsion angles α' ([AP]dG6(N^9)-[AP]dG6(C^8)-[AP]-(N)-[AP](C^1)) and β' ([AP]dG6(C^8)-[AP](N)-[AP](C^1)-[AP]-(C^{10A})) were each started at 0°, 90°, 180°, and 270° in all combinations, and the DNA starting conformation was the B-form except for a *syn* ($\chi = 60°$) glycosidic torsion for the [AP]dG6 residue as required by the experimental ^{13}C chemical shift data. These 16 trials represent arbitrary unbiased high-energy starting orientations of the carcinogen that equally survey the potential energy surface of the adduct. Furthermore, searching orientation space at 90° intervals of α' and β' is a robust procedure for locating all the important potential energy wells because our minimization protocol permits torsion angle variations of up to 100° in each minimization step (Hingerty et al., 1989). Consequently, energy minima in each quadrant of α' and β' are equally accessible, and the reduced variable domain of torsion angle space greatly enhances the likelihood of finding the important structures. In these trials, the DUPLEX hydrogen-bond penalty function (Hingerty et al., 1989) for Watson−Crick base pairing was utilized at the dT4·dA19, dC5·dG18, dC7·dG16, and dT8·dA15 base pairs, since the NMR data indicated that these hydrogen bonds were present.

Of the 16 computed conformations of the d(T4-C5-[AP]-G6-C7-T8)·d(A15-G16-C17-G18-A19) segment, one conformation had the lowest energy and very low goodness-of-fit indices. This conformation had energy of −212.1 kcal/mol and goodness-of-fit values for eqs 1 and 2 of 3.0 and 1.4, respectively, with $W = 15$ kcal/mol Å^2. The second- and third-ranked conformations had energies of −210.7 and −202.7 kcal/mol and goodness-of-fit indices for eq 1 of 3.0 and 0.7, respectively, and for eq 2 of 4.2 and 2.4, respectively. A superpositioned view of the d(T4-C5-[AP]G6-C7-T8)·(A15-G16-C17-G18-A19) segment of these three conformations is plotted in Figure 7. The d(T4-C5-[AP]G6-C7-T8)·d(A15-G16-C17-G18-A19) segment of the lowest energy structure was employed in building the [AP]dG·dC 11-mer duplex. For this purpose, an unmodified energy-minimized B-form dG·dC 11-mer duplex was first computed. The d(T4-C5-[AP]G6-C7-T8)·d(A15-G16-C17-G18-A19) segment was then embedded in the dG·dC 11-mer duplex by replacement with residues dT4, dC5, dG6, dC7, and dT8 and

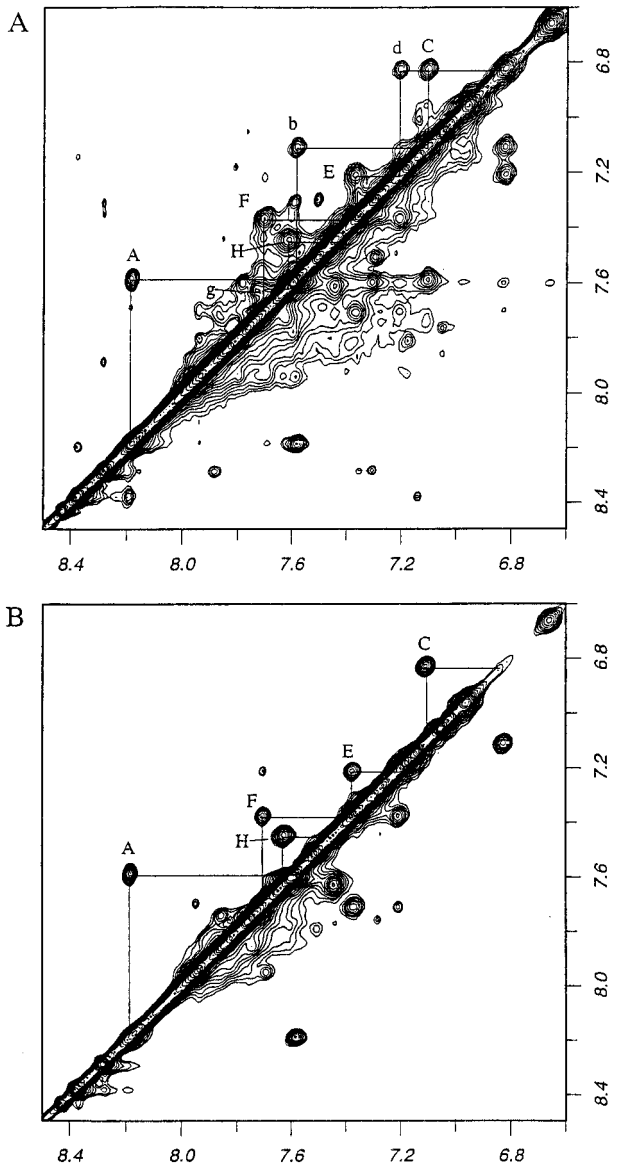

FIGURE 5: (A) Expanded NOESY (300 ms mixing time) contour plot of the [AP]dG·dC 11-mer duplex in D_2O buffer at 25 °C showing NOEs between the AP protons. (B) Expanded TOCSY (40 ms spin-lock time) contour plot of the [AP]dG·dC 11-mer duplex in D_2O buffer at 25 °C establishing coupling connectivities between the AP protons. The cross-peaks A−H are labeled as follows: A, AP(H2)-AP(H3); b, AP(H3)-AP(H4); C, AP(H4)-AP(H5); d, AP(H5)-AP(H6); E, AP(H6)-AP(H7); F, AP(H7)-AP(H8); g, AP(H8)-AP(H9); H, AP(H9)-AP(H10). Peaks labeled with capital letters represent through-bond coupling connectivities and are present in both NOESY and TOCSY spectra. Peaks labeled with lower case letters represent through-space connectivities and are only present in NOESY spectra. The chemical shift values (ppm) for the aminopyrene protons are as follows: AP(H2), 8.19; AP(H3), 7.59; AP(H4), 7.10; AP(H5), 6.82, AP(H6), 7.21; AP(H7), 7.37; AP(H8), 7.71; AP(H9), 7.62; AP(H10), 7.45.

their partners dA15, dG16, dC17, dG18, and dA19, followed by energy minimization with restraints. Subsequently, the hydrogen-bond penalty function and the distance restraints were released with energy minimization in one step, yielding a final unrestrained minimum energy conformation of the [AP]dG·dC 11-mer duplex.

Solution Structure. A view normal to the helix axis and looking into the major groove of the central d(T4-C5-[AP]-G6-C7-T8)·d(A15-G16-C17-G18-A19) segment of the NMR energy-minimized structure of the [AP]dG·dC 11-mer duplex is shown in Figure 8A. The corresponding structure for the entire adduct duplex is shown in supplementary Figure S2. The [AP]dG6 and dC17 moieties, drawn as darkened bonds, clearly demonstrate intercalation of the AP ring into the helix between the dC5·dG18 and dC7·dG16 base pairs. This results in a disruption of the alignment of the [AP]dG6 and dC17 such that both the modified deoxyguanosine and its partner deoxycytidine are displaced toward the major groove. The major groove edge of the dC5 is positioned over the deoxyguanosine base plane of [AP]dG6 (Figure 8B) with the latter tilted relative to the base pair planes in the adduct duplex (Figure 8A). The long axis of the intercalated pyrenyl ring is approximately parallel to the long axis of the flanking base pairs (Figure 8B).

Table 2: Comparison of Input Carcinogen−DNA Distance Bounds for the d(C5-[AP]G6-C7)·d(G16-C17-G18) with Those Observed for the Unrestrained Solution Conformation of the [AP]dG·dC 11-Mer Duplex

	carcinogen−DNA distance	
	exptl bounds	obsd bounds
exchangeable protons		
C5(NH_2-4b)−AP(H3)	3.5−5.5	3.73
G16(NH1)−AP(H8)	4.0−5.5	4.37
G16(NH1)−AP(H10)	4.0−5.5	5.51
G18(NH1)−AP(H2)	4.0−5.5	3.83
G18(NH1)−AP(H3)	4.0−5.5	5.27
nonexchangeable protons		
[AP]G6(H1′)−AP(H2)	>4.5	5.11
[AP]G6(H1′)−AP(H10)	2.2−3.6	3.28
G16(H2′)−AP(H5)	4.5−6.0	4.8
G16(H2′)−AP(H6)	4.0−6.0	4.6
G16(H2″)−AP(H5)	4.0−6.0	4.83
G16(H2″)−AP(H6)	4.0−6.0	3.81
C17(H4′)−AP(H6)	3.5−6.0	2.87

The carcinogen−base linkage site for the [AP]dG6 residue is defined by the torsion angles α′([AP]dG6(N^9)-[AP]dG6-(C^8)-[AP](N)-[AP](C^1)) = 209° and β′ ([AP]dG6(C^8)-[AP]-(N)-[AP](C^1)-[AP](C^{10A})) = 141°. The glycosidic torsion angles, sugar puckers, and backbone torsion angles for the d(T4-C5-[AP]G6-C7-T8)·d(A15-G16-C17-G18-A19) segment of the [AP]dG·dC 11-mer duplex are listed in supplementary Table S5. The following torsion angles deviate from standard B-DNA values. At the [AP]dG6 residue, the glycosidic torsion angle is 62°, in the *syn* domain, and the pseudorotation parameter, *P*, describing the sugar pucker is 103°, corresponding to a C1′-*exo*−O4′-*endo* conformation. In addition, at the partner dC17 residue, the glycosidic torsion angle is 318°, in the high *anti* region, compared to normal B-DNA values centered at about 240°, and the O3′-P torsion angle ξ is in the *trans* domain at 161° rather than the normal *gauche minus* centered at about 255°. Other torsion angles and pseudorotation parameters adopt typical B-DNA values.

DISCUSSION

Spectral Quality. The exchangeable and nonexchangeable proton NMR spectra of the [AP]dG·dC 11-mer duplex (Figure 1A and B, respectively) are of sufficient quality to have allowed us to undertake a structural characterization of the conformation at and adjacent to the [AP]dG lesion site. This analysis was not straightforward due to the somewhat broadened proton resonances for the d(T4-C5-[AP]G6-C7-T8)·d(A15-G16-C17-G18-A19) segment and our inability to assign the sugar protons of G18 and the NH

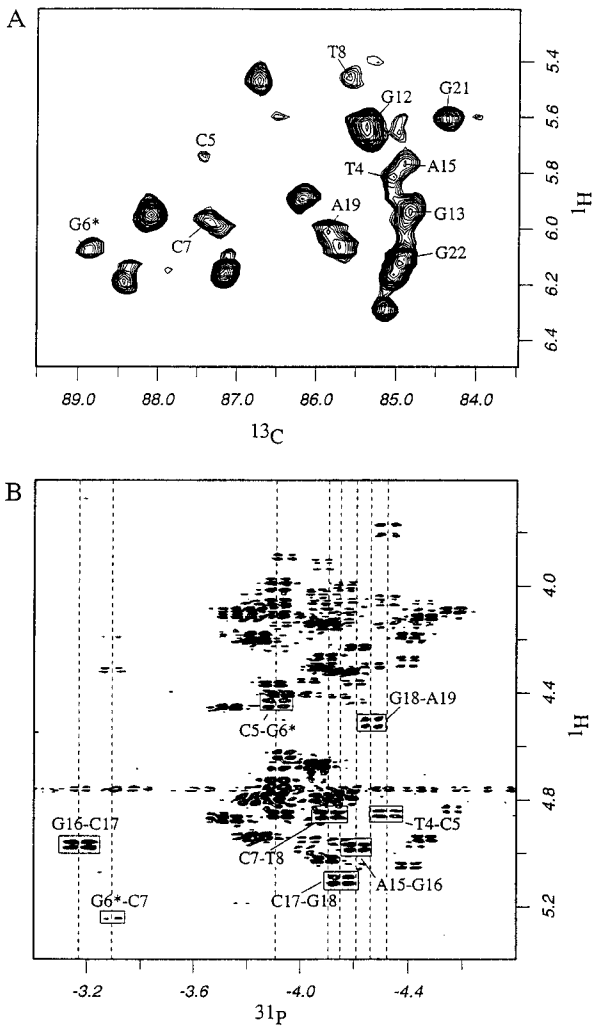

FIGURE 6: (A) Expanded contour plot of the ^{1}H−^{13}C heteronuclear multiple-quantum coherence (HMQC) experiment on the [AP]dG·dC 11-mer duplex in D_2O buffer at 25 °C. The H1′/C1′ assignments are marked for residues in the d(T4-C5-[AP]G6-C7-T8)·d(A15-G16-C17-G18-A19) segment. (B) Expanded contour plot of the proton-detected phosphorus−proton heteronuclear correlation experiment on the [AP]dG·dC 11-mer duplex in D_2O buffer at 25 °C. The phosphorus assignments are listed for steps centered about the lesion site. The correlation cross-peaks between the phosphorus and its 5′-flanking sugar H3′ protons are boxed.

proton associated with the [AP]dG covalent linkage site in the adduct duplex. The broadening of proton resonances centered about the [AP]dG adduct site has resulted in the observation of weak intermolecular NOEs which in turn have yielded distance restraints that can only be defined by wide bounds. Nevertheless, the present NMR study has defined the conformational consequences associated with the incorporation of a single [AP]dG adduct in an 11-mer duplex; the resulting NMR energy-minimized structure, which satisfies the NOE restraints and the chemical shift patterns, represents the predominant conformation.

NOE and Chemical Shift Patterns in the [AP]dG·dC 11-Mer. The solution conformation of the central segment of the [AP]dG·dC 11-mer duplex shown in Figure 8 establishes that the covalently attached aminopyrene ring intercalates between intact Watson−Crick dC5·dG18 and dC7·dG16 base pairs and displaces the dC17 positioned opposite the modified deoxyguanosine toward the major groove. Further, the deoxyguanosine ring of [AP]dG6 adopts a *syn* alignment and is positioned in the major groove, adopting a slightly tilted

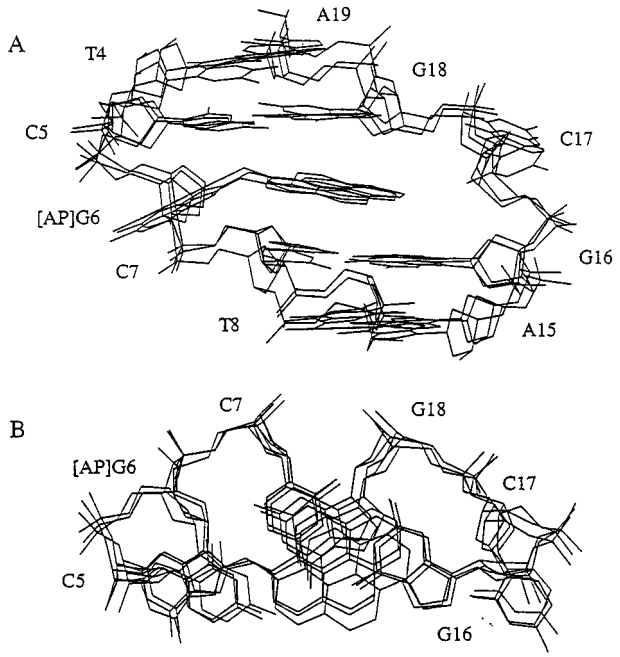

FIGURE 7: Superposition of the three d(C5-[AP]G6-C7)·d(G16-C17-G18) segments of the computed structures that best fit the NMR data of the [AP]dG·dC 11-mer duplex. These were obtained from the 16 trials which searched conformational space using the program DUPLEX and were guided by the NMR-based carcinogen−DNA restraints (Table 2). (A) View looking into the major groove and normal to the helix axis of the central segment. (B) View looking down the helix axis of the central segment.

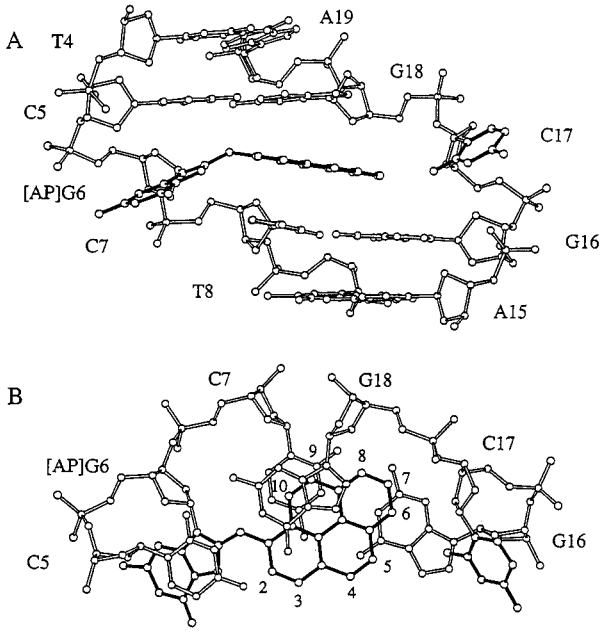

FIGURE 8: (A) View looking into the major groove and normal to the helix axis of the central d(T4-C5-[AP]G6-C7-T8)·d(A15-G16-C17-G18-A19) segment of the [AP]dG·dC 11-mer duplex solution structure. The AP ring system is shown in darkened bonds and is intercalated between the dC5·dG18 and dC7·dG16 base pairs. The modified dG6 and its partner dC17 bases are displaced into the major groove. (B) View looking down the helix axis for the d(C5-[AP]G6-C7)·d(G16-C17-G18) segment in the solution structure of the [AP]dG·dC 11-mer duplex. Figures were prepared using Molscript VI.1 (Kraulis, 1991).

orientation relative to adjacent base pair planes. This unusual structural alignment results in novel NOE and chemical shift patterns distinct from those observed for unperturbed helices.

Intercalation of the aromatic pyrenyl ring of the [AP]dG6 is supported by the large experimentally observed upfield shifts of the imino protons of dG16 (−1.20 ppm) and dG18 (−1.16 ppm), as well as the amino protons of dC7 (−0.56 and −0.44 ppm for the hydrogen-bonded and exposed protons, respectively) and dC5 (−0.43 ppm for the hydrogen-bonded proton) on proceeding from the control 11-mer to the [AP]dG·dC 11-mer duplex (Table S2). The intercalation of the AP ring is further supported by the observation of NOEs between the AP(H2), AP(H3), AP(H8), and AP(H10) protons and the imino protons of dG16 and dG18 in the adduct duplex (Table 2).

The alignment of the C^5-C^6-C^7-containing edge of the AP ring toward the d(G16-C17-G18) segment of the unmodified strand (Figure 8B) is consistent with the observed intermolecular NOEs between the AP(H5) and AP(H6) protons and the sugar protons of dG16 and dC17 in the adduct duplex (Table 2). Moreover, the alignment of the C^9-C^{10}-containing edge toward the [AP]dG6 base (Figure 8B) is consistent with the observed NOE between the AP(H10) proton and the sugar H1′ proton of [AP]dG6 in the adduct duplex (Table 2). The dC5·dG18 and dC7·dG16 base pairs maintain Watson−Crick alignment as established by the presence of interstrand cross-peaks between the upfield-shifted dG16 and dG18 imino protons and the amino protons of dC5 and dC7, respectively (peaks A, A′ and B, B′, Figure 2A) in the adduct duplex.

The glycosidic torsion angle (62°) of the modified deoxyguanosine in the [AP]dG·dC 11-mer duplex is in the *syn* domain. The standard approach for distinguishing *syn* from *anti* deoxyguanosine glycosidic torsion angles on the basis of magnitude of the NOE between the deoxyguanosine H8 proton and its own sugar H1′ proton (Patel, et al., 1982) cannot be used for the [AP]dG6 residue since the H8 proton is replaced by the aminopyrene ring. However, the [AP]-dG6 glycosidic torsion angle was assigned to the *syn* range based on the C1′ carbon of this modified deoxyguanosine which was shifted downfield by ∼3 ppm from the corresponding chemical shifts of other deoxyguanosine residues in the adduct duplex. Such a large C1′ deoxyguanosine downfield shift cannot result solely from ring current contributions and instead has been identified with *syn* glycosidic torsion angles for residues in the C2′-*endo* sugar pucker range (Greene, et al., 1995; Mao et al., 1995a,b). The identification of a *syn* glycosidic torsion angle for [AP]dG6 is also supported by the unusual downfield chemical shift (3.51 ppm) for the H2′ proton of this modified residue. Similar downfield shifts of the H2′ proton were detected for *syn* deoxyguanosine alignments in related adduct duplex systems (Norman et al., 1989; Kouchakdjian et al., 1989; Mao et al., 1995a,b; Cosman et al., 1995c).

The intercalation of the aminopyrenyl ring results in the displacement of the modified deoxyguanosine ring into the major groove (Figure 8A). The base plane of the displaced modified deoxyguanosine is somewhat tilted relative to the planes of the flanking dG·dC base pairs such that one face stacks over the base and sugar major groove edges of the 5′-flanking dC5 residue (Figure 8B) while the other face is exposed to solvent (Figure 8A). Such an alignment could account for the experimentally observed upfield shifts of the major groove base (H6) and sugar (H2′ and H3′) protons of dC5 (Table S2) since these nonexchangeable protons are positioned over the modified guanine ring of [AP]dG6 and are shifted upfield due to ring current contributions. We did not observe the imino proton of [AP]dG6 in the proton spectrum of the adduct duplex, consistent with the exposed alignment of this exchangeable proton in the structure of the [AP]dG·dC 11-mer duplex (Figure 8). The sugar H1′, H2′, and H3′ protons of [AP]dG6 are downfield relative to the same sugar protons for the control 11-mer duplex (Table S2), consistent with displacement of the modified deoxyguanosine out of the helix.

We observe downfield shifts for the base and sugar protons (Tables 1 and S2) of dC17 in the NOESY spectra (Figure 3) of the adduct duplex. This can be readily explained by the solution structure (Figure 8) in which the dC17 base is displaced out of the helix, positioned in the major groove, and does not stack with flanking dG·dC base pairs. The precise alignment of d(G16-C17-G18) is poorly defined by the NMR data due to the broadened linewidths for some of the resonances involving the dG16, dC17, and dG18 residues (Figure 3) in the adduct duplex. This result suggests that the [AP]dG adduct probably induces greater conformational heterogeneity at the looped out dC17 residue within the d(G16-C17-G18) segment on the unmodified strand when compared with the same segment in the control 11-mer.

Comparison of Base-Displaced Intercalated Conformations of [AP]-C^8-dG with [BP]-N^2-dG and [AF]-C^8-dG Adducts. We have reported base-displaced intercalation solution structures of (+)-*trans-anti*-[BP]-N^2-dG·single deletion (Cosman et al., 1994a), (+)-*cis-anti*-[BP]-N^2-dG·dC (Cosman et al., 1993a), (+)-*cis-anti*-[BP]-N^2-dG·single deletion (Cosman et al., 1994b), [AF]-C^8-dG·single deletion (Mao et al., 1995a), and [AF]-C^8-dG·double deletion (Mao et al., 1995b) adducts in the identical sequence context on the modified strand. The key difference between these adducts is that the benzo[*a*]pyrenyl ring is covalently linked through the N^2-exocyclic amino group of deoxyguanosine while the aminofluorene and aminopyrene rings are covalently linked through the C^8 position of deoxyguanosine.

There are similarities in the structural motifs determined for these adducts at the oligomer duplex level despite the pronounced differences in the covalent linkage site position. In all cases, the aromatic chromophores intercalate into the helix between flanking intact dG·dC base pairs. This is accompanied by displacement of the modified guanine into the major or minor groove in all cases and displacement of the partner dC into the major groove in the cases of (+)-*cis-anti*-[BP]-N^2-dG·dC (Cosman et al., 1993a) and [AP]-C^8-dG·dC (this study) adduct duplexes. These base-displaced intercalation structures in which the intercalation pocket is generated by displacing the modified base and its partner are to be contrasted with classical intercalation of covalently modified duplexes. In these structures, all base pairs are intact and the aromatic moiety slides between base pairs either 3′ or 5′ to the lesion site, by stretching and unwinding the helix, to form an intercalation pocket. Such classical intercalation structures have been observed in covalent adenine adducts of benzo[*c*]phenanthrene diol epoxides (Cosman et al., 1993b, 1995b) and benzo[*a*]pyrene diol epoxides (Schurter et al., 1995a,b; Yeh et al., 1996; Zegar et al., 1996).

Two significant differences are observed between the N^2-dG and C^8-dG adducts. (1) Both the [AP]-C^8-dG adduct opposite dC (this study) and [AF]-C^8-dG adduct opposite single- and double-deletion sites (Mao et al., 1995a,b) adopt

syn glycosidic torsion angles at the modified deoxyguanosine in contrast to the *anti* glycosidic torsion angle at the [BP]-N^2-dG adduct opposite dC and deletion sites. (2) The long axes of the intercalated AF (Mao et al., 1995a,b) and AP (this study) rings are parallel to that of the flanking dG·dC base pairs, in contrast to the orthogonal alignment of the long axis of the intercalated BP ring and flanking dG·dC base pairs (Cosman et al., 1993, 1994a,b).

There are some differences between the structures for [AF]-dG positioned opposite deletion sites (Mao et al., 1995a,b) and for [AP]dG positioned opposite dC (this study) which could reflect the contributions from having a residue or lack of it opposite the C^8-dG adduct site. More specifically, the base-displaced modified deoxyguanosine of [AF]dG positioned opposite −1 and −2 delection sites (Mao et al., 1995a,b) is tilted toward the 5′-side of the modified strand while the base-displaced modified deoxyguanosine of [AP]-dG positioned opposite dC is tilted, to a lesser extent, toward the 3′-side of the modified strand (Figure 8A). Another distinction between the two families of C^8-modified dG adduct duplexes is that dC7 and dG18 from partner strands are positioned over each other in the [AP]dG·dC adduct duplex (Figure 8B) but not in the [AF]dG·single deletion adduct duplex (Mao et al., 1995a).

Biological Significance. In *Escherichia coli* and *Salmonella typhimurium* 1-NP induces frame-shift mutations although base substitutions have also been detected at a low frequency (Rosenkranz & Mermelstein, 1983; Stanton et al., 1988). In these systems, 1-NP forms multiple DNA adducts (Herreno-Saenz et al., 1995). However, when [AP]dG was introduced in DNA as the major damage and template DNA was allowed to be replicated *in vivo*, frame-shift mutations occurred at a high frequency (Melchoir et al., 1994; Malia & Basu, 1995). A major fraction of the mutagenesis in *E. coli*, specifically one-base deletions and insertions, occurred in 5′-CG, 5′-GC, and 5′-GG sequences (Malia & Basu, 1995). Furthermore, a recent site-specific study established unambiguously that [AP]dG can cause −2 and +1 frame-shifts in a repetitive CpG sequence in *E. coli* (Malia et al., 1996). Therefore, our structural study in the CGC sequence context relates to major mutagenic hot spots induced by [AP]dG in bacteria.

Frame-shift mutagenesis is believed to occur as a result of misaligned structures which may be stabilized by intercalation of planar aromatic moieties (Streisinger et al., 1966; Drake & Baltz, 1976). In recent years a number of detailed, sequence-dependent mechanisms have been developed and applied to mutagenic hot spots of carcinogen-modified DNAs (Kunkel, 1990; Schaaper et al., 1990; Lambert et al., 1992; Garcia et al., 1993; Shibutani & Grollman, 1993; Napolitano et al., 1994). In these mechanisms it is envisioned that the polymerase stalls near the damaged base, permitting time for a rearrangement in which an unopposed bulge can form at the lesion site if the sequence is appropriate. The present [AP]dG opposite dC structure shares the feature of base-displacement intercalation with a number of other solution structures in which the carcinogen-modified base is at a deletion site: the (+)-*trans-anti*- and (+)-*cis-anti*-N^2-dG benzo[*a*]pyrene diol epoxide adducts at −1 deletion sites (Cosman et al., 1994a,b) and the [AF]dG adduct at −1 and −2 deletion sites (Mao et al., 1995a,b). These structures, together, emphasize that polycyclic aromatic carcinogens can stabilize extended bulged frame-shift intermediates by base-displacement intercalation. However, the current [AP]dG opposite dC structure stabilizes a conformation of this type without the context of a deletion site, in common with the [AAF]dG opposite dC structure (O'Handley et al., 1993) and one of the two coexisting [AF]dG·dC conformers (Cho et al., 1994; Eckel & Krugh, 1994) but unlike the (+)-*trans-anti* benzo[*a*]pyrene diol epoxide N^2-dG·dC adduct (Cosman et al., 1992). It is tempting to speculate that the stability of the base-displacement intercalation structure in the present [AP]dG duplex, even in the presence of the normal partner dC, relates to its high propensity to induce frame-shift mutations. In this respect, the [AP]dG adduct most resembles [AAF]dG, with both sharing the most marked preference for frame-shift mutations (Heflich & Neft, 1994) and adopting exclusively base-displaced intercalated structures in the d(C-G-C)·(G-C-G) sequence context. The solution structure presented in this work is the first experimental molecular view of the [AP]dG adduct incorporated in a DNA duplex. Future studies should reveal whether a similar type of structure is also observed in the context of a bulged duplex that models a frame-shift intermediate.

ACKNOWLEDGMENT

We thank Marazban Dehnugara for his technical assistance on this project.

SUPPORTING INFORMATION AVAILABLE

Four tables listing exchangeable and nonexchangeable proton chemical shifts for the entire [AP]dG·dC 11-mer adduct duplex, proton chemical shift differences on adduct formation, and backbone torsion angles for the central segment of the energy-minimized structure of the [AP]dG·dC 11-mer duplex and two figures showing intermolecular NOEs and the unrestrained structure of the entire [AP]-dG·dC 11-mer duplex (9 pages). Ordering information is given on any current masthead page.

REFERENCES

Abuaf, P., Hingerty, B. E., Broyde, S., & Grunberger, D. (1995) *Chem. Res. Toxicol. 8*, 369−378.

Altona, C., & Sundaralingam, M. (1972) *J. Am. Chem. Soc. 94*, 8205−8212.

Arnott, S., Bond, P. J., Selsing, E., & Smith, P. J. (1976) *Nucleic Acids Res. 2*, 2459−2470.

Bax, A., & Subramanian, J. (1986) *J. Magn. Reson. 67*, 565−570.

Beland, F. A., & Kadlubar, F. F. (1985) *Environ. Health Perspect. 62*, 19−30.

Beland, F. A., & Kadlubar, F. F. (1990) in *Handbook of Experimental Pharmacology, Vol. 94/I: Chemical Carcinogenesis and Mutagenesis* (Cooper, C. S., & Grover, P. L., Eds.) pp 267−325, Springer-Verlag, Heidelberg.

Bichara, M., & Fuchs, R. P. P. (1985) *J. Mol. Biol. 183*, 341−351.

Cho, B. P., Beland, F. A., & Marques, M. M. (1992) *Biochemistry 31*, 9587−9602.

Cho, B. P., Beland, F. A., & Marques, M. M. (1994) *Biochemistry 33*, 1373−1384.

Cosman, M., de los Santos, C., Fiala, R., Hingerty, B. E., Singh, S. B., Ibanez, V., Margulis, L. A., Live, D., Geacintov, N. E., Broyde, S., & Patel, D. J. (1992) *Proc. Natl. Acad. Sci. U.S.A. 89*, 1914−1918.

Cosman, M., de los Santos, C., Fiala, R., Hingerty, B. E., Ibanez, V., Luna, E., Harvey, R., Geacintov, N. E., Broyde, S., & Patel, D. J. (1993a) *Biochemistry 32*, 4145−4155.

Cosman, M., Fiala, R., Hingerty, B. E., Laryea, A., Lee, H., Harvey, R., Amin, S., Geacintov, N. E., Broyde, S., & Patel, D. J. (1993b) *Biochemistry 32*, 12488−12497.

Cosman, M., Fiala, R., Hingerty, B. E., Amin, S., Geacintov, N. E., Broyde, S., & Patel, D. J. (1994a) *Biochemistry 33*, 11507−11517.
Cosman, M., Fiala, R., Hingerty, B. E., Amin, S., Geacintov, N. E., Broyde, S., & Patel, D. J. (1994b) *Biochemistry 33*, 11518−11527.
Cosman, M., Xu, R., Hingerty, B. E., Amin, S., Harvey, R. G., Geacintov, N. E., Broyde, S., & Patel, D. J. (1995a) *Biochemistry 34*, 6247−6260.
Cosman, M., Laryea, A., Fiala, R., Hingerty, B. E., Amin, S., Geacintov, N. E., Broyde, S., & Patel, D. J. (1995b) *Biochemistry 34*, 1295−1307.
Cosman, M., Hingerty, B. E., Geacintov, N. E., Broyde, S., & Patel, D. J. (1995c) *Biochemistry 34*, 15334−15350.
de los Santos, C., Cosman, M., Hingerty, B. E., Ibanez, V., Margulis, L. A., Geacintov, N. E., Broyde, S., & Patel, D. J. (1992) *Biochemistry 31*, 5245−5252.
Drake, J. W., & Baltz, R. W. (1976) *Annu. Rev. Biochem. 45*, 11−37.
Eckel, L. M., & Krugh, T. R. (1994) *Biochemistry*, *33*, 13611−13624.
El-Bayoumy, K. (1992) *Chem. Res. Toxicol. 5*, 585−590.
Fuchs, R. P. P., & Daune, M. (1971) *FEBS Lett. 34*, 295−298.
Fuchs, R. P. P., Schwartz, N., & Daune, M. P. (1981) *Nature 294*, 657−659.
Fuchs, R. P. P., Schwartz, N., & Daune, M. P. (1983) *Environ. Health Perspect. 49*, 135−140.
Garcia, A., Lambert, I. B., & Fuchs, R. P. P. (1993) *Proc. Natl. Acad. Sci. U.S.A. 90*, 5989−5993.
Ghose, R., Marino, J. P., Wiberg, K. B., & Prestegard, J. H. (1994) *J. Am. Chem. Soc. 116*, 8827−8828.
Greene, K. L., Wang, Y., & Live, D. (1995) *J. Biomol. NMR 5*, 333−338.
Grunberger, D., Nelson, J. H., Cantor, C. R., Weinstein, I. B. (1970) *Proc. Natl. Acad. Sci. U.S.A. 66*, 488−494.
Heflich, R. H., & Neft, R. E. (1994) *Mutat. Res.: Rev. Genet. Toxicol. 318*, 73−174.
Heflich, R. H., Howard, P. C., & Beland, F. A. (1985) *Mutat. Res. 149*, 25−32.
Herreno-Saenz, D., Evan, F. E., Beland, F. A., & Fu, P. P. (1995) *Chem. Res. Toxicol. 8*, 269−277.
Hingerty, B. E., Figueroa, S., Hayden, T., & Broyde, S. (1989) *Biopolymers 28*, 1195−1222.
Hirose, M., Lee, M.-S., Wang, C. Y., & King, C. M. (1984) *Cancer Res. 44*, 1158−1162.
Howard, P. C., & Beland, F. A. (1982) *Biochem. Biophys. Res. Commun. 104*, 727−732.
Howard, P. C., Beland, F. A., & Cerniglia, C. E. (1983) *Carcinogenesis, 4*, 985−990.
Howard, P. C., Heflich, R. H., Evans, F. E., & Beland, F. A. (1983) *Cancer Res. 43*, 2052−2058.
International Agency for Research on Cancer (1989) Diesel and Gasoline Engine Exhausts and Some Nitroarenes, in *IARC Monographs on the Evaluation of Carcinogenic Risk to Humans*, Vol. 39, pp 1−458, IARC, Lyon, France.
Kouchakdjian, M., Marinelli, E., Gao, X. L., Johnson, F., Grollman, A., & Patel, D. J. (1989) *Biochemistry 28*, 5647−5657.
Kraulis, P. J. (1991) *J. Appl. Crystallogr. 24*, 946−950.
Kunkel, T. A. (1990) *Biochemistry 29*, 8003−8011.
Lambert, I. P., Napolitano, R. L., & Fuchs, R. P. P. (1992) *Proc. Natl. Acad. Sci. U.S.A. 89*, 1310−1314.
Malia, S. A., & Basu, A. K. (1995) *Biochemistry 34*, 96−104.
Malia, S. A., Vyas, R. R., & Basu, A. K. (1996) *Biochemistry 35*, 4568−4577.
Mao, B., Cosman, M., Hingerty, B. E., Broyde, S., & Patel, D. J. (1995a) *Biochemistry 34*, 6226−6238.
Mao, B., Hingerty, B. E., Broyde, S., & Patel, D. J. (1995b) *Biochemistry 34*, 16641−16653.
Melchior, W. B., Jr., Marques, M. M., & Beland, F. A. (1994) *Carcinogenesis 15*, 889−899.
Napolitano, R. L., Lambert, I. B., & Fuchs, R. P. P. (1994) *Biochemistry 33*, 1311−1315.
Newton, R. K., Mittelstaedt, R. A., Manjanantha, M. G., & Heflich, R. H. (1992) *Carcinogenesis 13*, 819−825.
Nolan, S. J., Vyas, R. R., Hingerty, B. E., Ellis, S., Broyde, S., Shapiro, R., & Basu, A. K. (1996) *Carcinogenesis 17*, 133−144.
Norman, D., Abuaf, P., Hingerty, B. E., Live, D., Grunberger, D., Broyde, S., & Patel, D. J. (1989) *Biochemistry 28*, 7462−7476.
O'Handley, F. F., Sanford, D. G., Xu, R., Lester, C. C., Hingerty, B. E., Broyde, S., & Krugh, T. R. (1993) *Biochemistry 32*, 2481−2497.
Ohnishi, Y., Kinouchi, T., Manabe, Y., Tsutsui, H., Otsuka, H., Tokiwa, H., & Otofuji, T. (1985) Nitro Compounds in Environmental Mixtures and Foods in *Short-Term Genetics Bioassays in the Evaluation of Complex Environmental Mixtures* (Waters, M. D., Shandhu, S. S., Lewtas, J., Claxton, L., Strauss, G., & Nesnow, S., Eds.) pp 195−204, Plenum Press, New York.
Patel, D. J., Kozlowski, S. A., Nordheim, A., & Rich, A. (1982) *Proc. Natl. Acad. Sci. U.S.A. 79*, 1413−1417.
Rosenkranz, H. S., McCoy, E. C., Sanders, D. R., Butler, M., Kiriazides, D. K., & Mermelstein, R. (1980) *Science 209*, 1039−1043.
Rosenkranz, H. S., & Mermelstein, R. (1983) *Mutat. Res. 114*, 217−267.
Rosenkranz, H. S., & Mermelstein, R. (1985) *J. Environ. Sci. Health C3*, 221−272.
Schaaper, R. M., Koffel-Schwartz, N., & Fuchs, R. P. P. (1990) *Carcinogenesis 11*, 1087−1095.
Schurter, E. J., Yeh, H. J. C., Sayer, J. M., Lakshaman, M. K., Yagi, H., Jerina, D. M., & Gorenstein, D. G. (1995a) *Biochemistry 34*, 1364−1375.
Schurter, E. J., Sayer, J. M., Oh-Hara, T., Yeh, H. J. C., Yagi, H., Luxon, B. A., Jerina, D. M., & Gorenstein, D. G. (1995b) *Biochemistry 34*, 9009−9020.
Shapiro, R., Hingerty, B. E., & Broyde, S. (1989) *J. Biomol. Struct. Dyn. 7*, 493−513.
Shibutani, S., & Grollman, A. P. (1993) *J. Biol. Chem. 268*, 11703−11710.
Singer, B., & Grunberger, D. (1983) *Molecular Biology of Mutagens and Carcinogens*, Plenum Press, New York.
Stanton, C. A., Chow, F. L., Phillips, D. H., Grover, P. L., Garner, R. C., & Martin, C. N. (1985) *Carcinogenesis 6*, 535−538.
Stanton, C. A., Garner, R. C., & Martin, C. N. (1988) *Carcinogenesis 9*, 1153−1157.
Streisinger, G., Okada, Y., Emrich, J., Newton, J., Tsugita, A., Tezaghi, E., & Inouye, M. (1966) *Cold Spring Harbor Symp. Quant. Biol. 31*, 77−84.
Taylor, E. R., & Olson, W. K. (1983) *Biopolymers 22*, 2667−2702.
Tokiwa, H., & Ohnishi, Y. (1986) *CRC Crit. Rev. Toxicol. 17*, 23−60.
van de Ven, F. J., & Hilbers, C. W. (1988) *Eur. J. Biochem. 178*, 1−38.
Vyas, R. R., Nolan, S. J., & Basu, A. K. (1993) *Tetrahedron Lett. 34*, 2247−2250.
Vyas, R. R., & Basu, A. K. (1995) *Carcinogenesis 16*, 811−816.
Yang, J.-L., Maher, V. M., & McCormick, J. J. (1988) *Mol. Cell. Biol. 8*, 3364−3372.
Yeh, H. J. C., Sayer, J. M., Liu, X., Altieri, A. S., Bird, R. A., Lakshman, M. K., Yagi, H., Schurter, E. J., Gorenstein, D. G., & Jerina, O. M. (1996) *Biochemistry* (in press).
Zegar, I. S., Kim, S. J., Johansen, T. N., Harris, C. M., Harris, T. M., & Stone, M. P. (1996) *Biochemistry* (in press).

BI961078O